

Controlling the spin orientation of photoexcited electrons by symmetry breaking

Lan Qing,* Yang Song, and Hanan Dery†

Department of Physics and Astronomy, University of Rochester, Rochester, New York 14627

We study reflection of optically spin-oriented hot electrons as a means to probe the semiconductor crystal symmetry and its intimate relation with the spin-orbit coupling. The symmetry breaking by reflection manifests itself by tipping the net-spin vector of the photoexcited electrons out of the light propagation direction. The tipping angle and the pointing direction of the net-spin vector are set by the crystal-induced spin precession, momentum alignment and spin-momentum correlation of the initial photoexcited electron population. We examine non-magnetic semiconductor heterostructures and semiconductor/ferromagnet systems and show the unique signatures of these effects.

PACS numbers: 72.25.Fe, 72.25.Mk, 72.25.Rb, 71.70.Ej

The intimate relation between the spin-orbit coupling of crystals and their symmetry is a theme of on-going research for more than a half-century [1–14]. The rapid progress of spintronics research has provided new powerful techniques to study this relation [15]. In semiconductors it is readily seen in the valence band energy dispersion [1, 2], in spin relaxation of electrons [3], or in optical selection rules [4, 5]. In magnetic materials this relation sets the magnetocrystalline anisotropy and magnetostriction constants [13, 14]. In this letter, we elucidate a novel phenomenon in bulk semiconductors that relies on intriguing manifestations of this relation: spin-momentum correlation and coherent spin precession of photoexcited electrons. We use symmetry breaking by reflection to store information from these ultrashort elusive processes into the net-spin vector of electrons. The information is encoded by tipping the net-spin vector away from the light propagation axis. Therefore, memory of ultrafast decaying coherent effects due to spin-orbit coupling and crystal symmetry is prolonged and lasts for ~ 1 ns rather than ~ 1 ps in bulk systems.

We first explain the correlation tipping phenomenon in a photoexcited direct gap semiconductor. Figure 1(a) shows the momentum alignment and spin-momentum correlation of electrons immediately after photoexcitation. The shown distributions are compactly derived by using the spherical model at the top of the valence band [1] and s -type states in the conduction band. The density matrix of photoexcited electrons is then [4],

$$\mathcal{D}(t, \mathbf{k}) = \left\{ \mathcal{I} + \frac{1}{2}\alpha(t)[3|\hat{\mathbf{e}} \cdot \hat{\mathbf{k}}|^2 - 1]\mathcal{I} + 2S(t)(\hat{\boldsymbol{\sigma}} \cdot \hat{\mathbf{p}}) + \frac{1}{2}\beta(t)[3(\hat{\boldsymbol{\sigma}} \cdot \hat{\mathbf{k}})(\hat{\mathbf{p}} \cdot \hat{\mathbf{k}}) - (\hat{\boldsymbol{\sigma}} \cdot \hat{\mathbf{p}})] \right\} F(t, k). \quad (1)$$

$\hat{\mathbf{k}}$ ($\hat{\mathbf{e}}$) is the unit vector in the direction of electron momentum (light polarization). $\hat{\boldsymbol{\sigma}}$ (\mathcal{I}) denotes the Pauli matrix vector (the 2×2 unit matrix). The photon angular momentum unit vector is defined by $\hat{\mathbf{p}} \equiv i\hat{\mathbf{e}} \times \hat{\mathbf{e}}^*$. For linearly polarized light $\hat{\mathbf{p}} = 0$ and for circularly polarized light, $|\hat{\mathbf{e}} \cdot \hat{\mathbf{k}}|^2 = [1 - (\hat{\mathbf{p}} \cdot \hat{\mathbf{k}})^2]/2$. The parameters α , S and β are, respectively, measures of momentum alignment, of average spin and of spin-momentum corre-

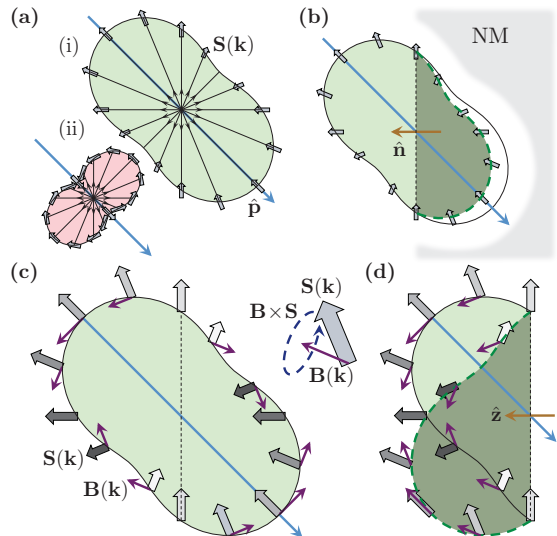


FIG. 1: (a) Momentum and spin distributions of photoexcited electrons following transitions with (i) heavy holes and (ii) light holes [16]. The length of a line from the center represents the relative population of excited electrons with momentum along the arrow's direction. The thick arrows on the edge line represent the correlated spins. (b) Correlation induced tipping by partial reflection. The net-spin vector is tipped away from the light propagation axis $\hat{\mathbf{p}}$ due to missing transmitted electrons with spins mostly along the interface normal $\hat{\mathbf{n}}$. (c) Spin precession of electrons immediately after photoexcitation. Electrons moving in opposite directions have the same initial spin direction but precess at opposite angles. (d) Precession induced tipping by complete reflection. The net-spin vector is tipped away from $\hat{\mathbf{p}}$ due to a rephasing effect (see text).

lation. $S(t)$ decays exponentially with the spin relaxation time from initial value $S_0 \approx -1/4$. $\alpha(t)$ and $\beta(t)$ decay exponentially with the much shorter momentum relaxation time from their initial values $\alpha_0 \approx \beta_0 \approx \pm 1$ [17]. The lower/upper sign is for transitions with heavy/light holes. Finally, $F(t, k)$ relates to the density of excited electrons. Figure 1(b) elucidates the correlation induced tipping effect for electrons that are generated with heavy holes. This effect is governed by transmission of electrons immediately after excitation (prior to the decay of $\beta(t)$).

in Eq. (1)). For example, consider electrons that propagate parallel and perpendicular to the reflection plane (shown in Fig. 1(b) by the two spins on the edges of the dash line and the two spins along $\pm\hat{\mathbf{n}}$). Their net spin is not collinear with $\hat{\mathbf{p}}$ due to missing electrons along $-\hat{\mathbf{n}}$. Similar explanation holds for other spin and momentum directions. The overall effect is that the net-spin vector changes from $S_0\hat{\mathbf{p}}$ to $S_0\hat{\mathbf{p}} - (c\hat{\mathbf{p}} \cdot \hat{\mathbf{n}})\hat{\mathbf{n}}$ where c is a measure of the transmission amplitude.

The second tipping phenomenon results from intrinsic spin precession of electrons in semiconductors without inversion symmetry [3]. The spin precession is due to a torque exerted by the electron's effective magnetic field whose components are $B_i \propto k_i(k_j^2 - k_m^2)$ where $\{k_i, k_j, k_m\}$ are the components of the electron wavevector along the crystallographic axes. Figure 1(c) shows the intrinsic spin precession of photoexcited electrons immediately after generation. Electrons that move in opposite directions have similar initial spin direction but precess at opposite angles. The net angle precession of the pair is zero on average. This picture is changed by specular reflection of one of the electrons off an interface as shown in Fig. 1(d). Here, k_z and B_z of an electron flip signs after specular reflection whereas its spin components $\{S_x, S_y, S_z\}$ remain unchanged. This causes S_x and S_y to 're-phase' to some degree due to the flip of B_z whereas S_z keeps its precession unperturbedly. The net effect is that transverse spin components with respect to the normal of the reflection plane decay slower than the longitudinal component. This effect is robust in both complete or partial reflection and it can be further amplified by multiple/opposite interface reflections. Scattering events reduce the magnitude of the net-spin vector but they do not change its direction. We will show that in spite of a notable Dyakonov-Perel spin relaxation of hot electrons the net-spin vector after momentum and energy relaxation remains measurable [18].

The time evolution of photoexcited electrons is studied by extensive Monte Carlo simulations (see [19] for technical details). The initial wavevector and spin directions are randomized according to the distributions in Eq. (1). The initial electron density follows the light attenuation profile. We use the effective mass approximation in calculating electron transport and quantum mechanical transmission probabilities across interfaces. Effective masses, band-gaps and band offsets are taken from Ref. [20]. Momentum and energy relaxations of hot electrons are simulated by the Fröhlich interaction [21]. Between scattering and reflection events the spin precesses about its intrinsic field. The simulation ends when electrons reach the bottom of the conduction band (typically after 1 ps). Spin relaxation at later times occurs on >1 ns time scales [12].

We first study the tipping effects in non-magnetic heterostructures. To distinguish between correlation and precession induced tipping we employ two setups of the

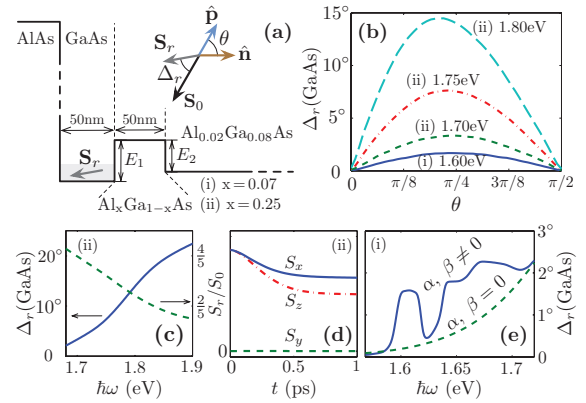


FIG. 2: (a) Simulated excitation geometry and heterostructure setups (i) and (ii). $\hat{\mathbf{n}}$ is along the z crystal axis. $\hat{\mathbf{p}}$ is in the x - z crystal plane ($\cos\theta = \hat{\mathbf{p}} \cdot \hat{\mathbf{n}}$). \mathbf{S}_r is the remained net-spin vector in the GaAs region after energy relaxation. Δ_r is the tipping angle of \mathbf{S}_r away from the optically injected spin direction. (b) Δ_r vs θ for various setups and photon energies. (c) Δ_r (left) and S_r (right) vs photon energy in setup (ii). The decay of \mathbf{S}_r is due to hot-electron relaxation [18]. (d) Spin evolution along crystal axes in the GaAs region in setup (ii). (e) Δ_r vs photon energy in setup (i) with/without alignment and correlation. (c)-(e) correspond to $\theta = \pi/4$.

heterostructure AlAs/GaAs(50 nm)/Al_xGa_{1-x}As(50 nm)/Al_{0.02}Ga_{0.98}As. The structure, shown in Fig. 2(a), ensures that electrons experience interface reflections during relaxation in the GaAs region. Confinement effects are negligible and all regions are bulk in nature. Setup (i) includes a shallow inner barrier ($x=0.07$) for which the potential steps are $E_1 = 63$ meV & $E_2 = 45$ meV (see Fig. 2(a)). For certain photon energies there is a favored net transmission from the GaAs region to the Al_{0.02}Ga_{0.98}As region. The spins of transmitted electrons are mostly aligned with the interface normal rather than the optically injected spin direction. Setup (ii) includes higher inner barrier ($x=0.25$) for which the potential steps are $E_1 = 230$ meV & $E_2 = 212$ meV. The tipping angle is governed by spin precession of hot electrons in the GaAs region prior to thermalization while bouncing back and forth from the potential walls. In both setups, quantum tunneling across the 50 nm inner barrier is negligible.

Figure 2(b) shows the dependence of the tipping angle on the light propagation direction for various photon energies. Δ_r is the tipping angle of the net-spin vector in the GaAs region after energy relaxation. θ is the angle between the photon angular momentum ($\hat{\mathbf{p}}$) and the interface normal ($\hat{\mathbf{n}}$) as shown in Fig. 2(a). We first focus on the results of setup (ii). The tipping angle is maximized when light propagates along the $\langle 101 \rangle$ & $\langle 011 \rangle$ crystallographic axes ($\theta = \pi/4$) due to the increased spin precession frequencies along these directions. Similarly, the tipping angles increase with photon energies due to the enhanced precession of electrons. Figure 2(c) shows

the tipping angle as a function of photon energy when $\theta = \pi/4$. We see that the magnitude of the net-spin vector after energy relaxation is measurable in all of the studied photon energy range. Figure 2(d) shows the time evolution of the net-spin along the crystallographic axes for $\theta = \pi/4$ and photon energy of 1.75 eV. The aforementioned ‘re-phasing’ effect is seen in the slower decay of S_x during the energy relaxation in the first 0.5 ps (the z component of the intrinsic field changes direction with each reflection). At later times (>1 ps) the precession frequency and spin relaxation are much slower.

Figure 2(e) shows correlation induced tipping angles as a function of photon energy when $\theta = \pi/4$. As a reference, we also simulate a case where momentum alignment and spin-momentum correlation are neglected (dash line). In the latter case, only spin precession during the initial coherent phase induces the tipping angle. The different results in Fig. 2(e) are a clear evidence of the correlation induced tipping. The first sharp increase is reached when electrons have enough energy to cross to the barrier region. The missing transmitted electrons have spin components mostly along $\hat{\mathbf{n}}$ (generated with heavy holes). The sudden drop is due to the emergence of transmitted hot electrons generated with light holes. It can be explained by the large difference in spin-momentum correlation of these two populations (see Fig. 1(a)). At higher energies the signal increases again due to transmission of electrons in a wider momentum range. Further increase of photon energy eventually suppresses this mechanism due to the increased precession rates.

Partial reflection off a ferromagnet provides unique signatures of momentum alignment and spin-momentum correlation that are interwoven with the magnetization direction of the ferromagnet. We perform detailed Monte Carlo simulations for the heterostructure in Fig. 3(a). It consists of Fe/GaAs(150 nm)/Al_{0.3}Ga_{0.7}As(50 nm)/Al_{0.25}Ga_{0.75}As(50 nm)/AlAs. For certain photon energies reflected hot electrons from the Fe/GaAs interface reach region I (Al_{0.25}Ga_{0.75}As) only if they do not experience energy relaxation in the GaAs region. In addition, the spins of these electrons do not precess in their short passage since their motion is along a crystallographic axis ($\hat{\mathbf{n}} = \hat{\mathbf{z}}$). Partial and spin selective reflection across the Fe/GaAs interface is modeled by a 0.5 eV high and 6 nm wide parabolic Schottky barrier [19]. Fermi wavevectors for majority and minority electrons in Fe are, respectively, 1.1 Å⁻¹ and 0.42 Å⁻¹ [22].

Figure 3(b) shows the tipping angle after energy relaxation in region I as a function of the photon energy. At photon energies just below the band-gap of region I, transmission from the GaAs into region I across the inner barrier is possible only for electrons that are generated with heavy-holes and that are directed along $\hat{\mathbf{n}}$. This is shown in the low energy side of Fig. 3(b). Since the spin direction of these electrons is parallel to their wavevector, the tipping angle is simply the angle between the

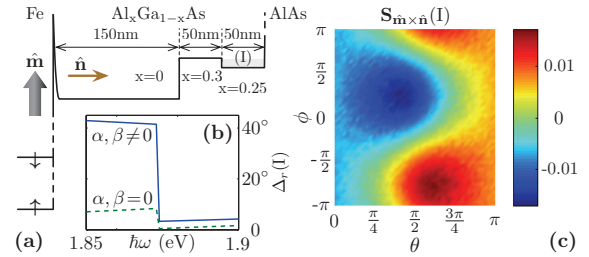


FIG. 3: (a) Simulated excitation geometry and heterostructure. $\hat{\mathbf{m}}$, $\hat{\mathbf{n}}$ and $\hat{\mathbf{m}} \times \hat{\mathbf{n}}$ are along crystallographic axes (in-plane magnetization). (b) Tipping angle of the relaxed net-spin vector in region I vs photon energy when the light propagation axis is 45° from $\hat{\mathbf{n}}$. The contribution of alignment and correlation are clearly seen. (c) Relaxed net-spin along $\hat{\mathbf{m}} \times \hat{\mathbf{n}}$ in region I versus light propagation direction (the photon energy is 1.85 eV). The polar (θ) and azimuthal (ϕ) angles are measured from $\hat{\mathbf{n}}$ and $\hat{\mathbf{m}} \times \hat{\mathbf{n}}$, respectively.

optically injected direction and $\hat{\mathbf{n}}$. The step occurs when electrons are photoexcited in region I and the net-spin becomes aligned with the optically injected spin direction (the transmitted electrons from the GaAs region are shadowed by the density of photoexcited electrons in region I). Figure 3(c) shows the relaxed spin component along $\hat{\mathbf{m}} \times \hat{\mathbf{n}}$ in region I as a function of the light propagation direction for photon energy of 1.85 eV. This relatively small component is an entwined signature of the ferromagnet and the spin-momentum correlation.

The simulated results in Figs. 2 & 3 are consistent with a simple quantitative analysis. In the spin precession case (setup (ii) in Fig. 2), a complete reflection brings about a $(\hat{\mathbf{p}} \cdot \hat{\mathbf{n}})\hat{\mathbf{n}} = \cos \theta \hat{\mathbf{n}}$ spin component after integrating the contributions from all electrons [19]. This term explains the $\sin 2\theta$ behavior of the tipping angle in Fig. 2(b). The coefficient of this term is quadratic in the intrinsic field and thus explains the build-up of the tipping angle while electrons are hot (see Fig. 2(d)). Spin-momentum correlation also presents a $\hat{\mathbf{p}} \cdot \hat{\mathbf{n}}$ amplitude dependence. If spin precession effects are small and photoexcited electrons reach the interface prior to momentum scattering (e.g., Fig. 3(a)) then the integrated net-spin vector after reflection from the ferromagnet reads,

$$\mathbf{S}_r = n_0 \ell S_0 \hat{\mathbf{p}} - n_0 \left\{ (4\lambda_0 S_0 + \delta_0^\beta) \hat{\mathbf{p}} - 3(\hat{\mathbf{p}} \cdot \hat{\mathbf{n}}) \delta_0^\beta \hat{\mathbf{n}} \right. \\ \left. + [\lambda_1 - \lambda_2 + \frac{1}{2}(1 - 3|\hat{\mathbf{e}} \cdot \hat{\mathbf{n}}|^2)(\delta_1^\alpha - \delta_2^\alpha)] \hat{\mathbf{m}} \right. \\ \left. - (4\lambda_3 S_0 + \delta_3^\beta) \hat{\mathbf{m}} \times \hat{\mathbf{p}} + 3(\hat{\mathbf{p}} \cdot \hat{\mathbf{n}}) \delta_3^\beta \hat{\mathbf{m}} \times \hat{\mathbf{n}} \right\}. \quad (2)$$

$\hat{\mathbf{m}} = 0$ denotes reflection off a non-magnetic material. ℓ is the inverse of light absorption coefficient and n_0 is the density of excited electrons. The λ and δ parameters are integration constants that depend on the transmission across the barrier where λ_i (δ_i) terms denote isotropic and uncorrelated (momentum aligned and spin correlated) contributions. The total reflection is spin independent and governed by λ_0 & δ_0^β terms, the spin selective

reflection by $(\lambda_1 - \lambda_2) \& (\delta_1^\alpha - \delta_2^\alpha)$ terms, and the magnetization induced torque by $\lambda_3 \& \delta_3^\beta$ terms. The α/β superscript indicates signatures of alignment/correlation. For detailed expressions of all terms see [19]. Previous experimental investigations of the ferromagnetic proximity effect [23, 24] and their ensuing theories [25–27] were focused on ferromagnetic signatures while ignoring the alignment and correlation of photoexcited electrons. In this view, Ciuti *et al.* have derived a reduced form of Eq. (2) in which $\delta_i^\alpha = \delta_i^\beta = 0$ [25]. Our analysis shows that in properly designed structures, correlation induced signatures are experimentally resolvable by the $\hat{\mathbf{p}} \cdot \hat{\mathbf{n}}$ amplitude dependence of the non-magnetic ($\hat{\mathbf{n}}$) and magnetic ($\hat{\mathbf{m}} \times \hat{\mathbf{n}}$) spin components.

Prolonged alignment and correlation signatures in semiconductors with inversion symmetry are possible by partial reflection. For example, in silicon the $\hat{\mathbf{k}}$ parameter in Eq. (1) is replaced with \mathbf{k}_0/k_0 where \mathbf{k}_0 denotes any of the six wavevectors at the valley centers along the Δ -axes. In addition, the values of α , β and S depend mainly on parameters of the dominant transverse-optical phonon assisted transition [6]. The alignment and correlation signatures would only be effective by reflection of electrons from valleys whose \mathbf{k}_0 is perpendicular to the normal of the interface. The reason is that tunneling with the five times heavier longitudinal component is exponentially less effective [28]. An intuitive effect is that for excitation by a linearly polarized light the ferromagnetic signature along $\hat{\mathbf{m}}$ is weaker if $|\hat{\mathbf{e}} \cdot \hat{\mathbf{n}}| = 1$ [29].

In conclusion, reflections off non-magnetic semiconductor heterojunctions and semiconductor/ferromagnet interfaces have been shown to be a powerful tool to study coherent effects of the crystal symmetry and spin-orbit coupling. Tipping the net-spin vector out of the optically injected direction is a measure of these effects. The predicted tipping angles are noticeable and can be probed, for example, via the photoluminescence of energy relaxed free excitons. The tipping angle corresponds to the angle at which the detected circular polarization is maximal. Tunable parameters are the photon energy and light propagation direction. The tipped net-spin vector would ultimately evolve in hyperfine interaction and polarize the nuclear spin system. In this case, ultrafast decaying coherent effects that result from the crystal symmetry and spin-orbit coupling can be inferred by NMR type signals of a $\sim 10^{10}$ slower interaction.

This work is supported by AFOSR Contract No. FA 9550-09-1-0493 and NSF Contract No. ECCS-0824075.

- [2] G. Dresselhaus, Phys. Rev. **100**, 580 (1955).
- [3] M. I. Dyakonov, V. I. Perel, Sov. Phys. JETP **33**, 1053 (1971); Sov. Phys. Solid State **13**, 3023 (1972).
- [4] V. D. Dymnikov, M. I. Dyakonov and N. I. Perel, Sov. Phys. JETP **44**, 1252 (1976).
- [5] *Optical Orientation*, edited by F. Meier and B. P. Zakharchenya (North-Holland, New York, 1984).
- [6] P. Li and H. Dery, Phys. Rev. Lett. **105**, 037204 (2010).
- [7] V. I. Zemskii, B. P. Zakharchenya, and D. N. Mirlin, JETP Lett. **24**, 82 (1976).
- [8] V. L. Alperovich, V. I. Belinicher, V. N. Novikov, and A. S. Terekhov, JETP Lett. **31**, 546 (1980).
- [9] Y. A. Bychkov and E. I. Rashba, J. Phys. C **17**, 6039 (1984).
- [10] R. D. R. Bhat and J. E. Sipe, Phys. Rev. Lett. **85**, 5432 (2000).
- [11] J. Wunderlich, B. Kaestner, J. Sinova and T. Jungwirth, Phys. Rev. Lett. **94**, 047204 (2005).
- [12] S. A. Crooker and D. L. Smith, Phys. Rev. Lett. **94**, 236601 (2005).
- [13] J. Kanamori, in *Magnetism*, edited by G. T. Rado and H. Suhl (Academic Press, New York, 1963), Vol. I, p. 127.
- [14] T. Dietl, H. Ohno, and F. Matsukura, Phys. Rev. B **63**, 195205 (2001).
- [15] I. Zutic, J. Fabian, and S. Das Sarma, Rev. Mod. Phys. **76**, 323 (2004).
- [16] The density of states implies that heavy-hole excitations are larger by about $[(m_h/m_l)(m_e + m_l)/(m_e + m_h)]^{1.5}$ than light-hole excitations where $m_{e,h,l}$ are the effective mass of electrons, heavy holes and light holes, respectively. In GaAs, for example, the ratio is about 2.
- [17] These values hold for photon energies in the $[E_g, E_g + \Delta]$ range where E_g is the band-gap and Δ is spin-orbit splitting of the valence band in the Γ -point.
- [18] Spin relaxation of hot electrons is due to direction and magnitude randomization of the k^3 -dependent intrinsic magnetic fields after scattering events (see Ref. [3]). The tipping angle shows a $(\hbar\omega - E_g)^3$ dependence where $\hbar\omega$ (E_g) is the photon (band-gap) energy.
- [19] See supplementary material for simulation procedures, for derivations of the $(\hat{\mathbf{p}} \cdot \hat{\mathbf{n}})\hat{\mathbf{n}}$ term and for the λ_i & δ_i terms in Eq. (2). It also provides details that support our calculation methods.
- [20] *Properties of Aluminum Gallium Arsenide*, edited by S. Adachi (INSPEC, London, 1993).
- [21] P. Y. Yu and M. Cardona, *Fundamentals of Semiconductors* (Springer, Berlin, 2005), Ch. 3.
- [22] J. C. Slonczewski, Phys. Rev. B **39**, 6995 (1989).
- [23] R. K. Kawakami, Y. Kato, M. Hanson, I. Malajovich, J. M. Stephens, E. Johnston-Halperin, G. Salis, A. C. Gossard, D. D. Awschalom, Science **294**, 131 (2001).
- [24] R. J. Epstein, I. Malajovich, R. K. Kawakami, Y. Chye, M. Hanson, P. M. Petroff, A. C. Gossard, and D. D. Awschalom, Phys. Rev. B **65**, 121202 (2002).
- [25] C. Ciuti, J. P. McGuire, and L. J. Sham, Phys. Rev. Lett. **89**, 156601 (2002).
- [26] G. E. Bauer, A. Brataas, Y. Tserkovnyak, B. I. Halperin, M. Zwierzycki, and P. J. Kelly, Phys. Rev. Lett. **92**, 126601 (2004).
- [27] V. N. Gridnev, JETP Lett. **77**, 187 (2003).
- [28] P. Mavropoulos, Phys. Rev. B **78**, 054446 (2008).
- [29] This is a result of preferential excitation in valleys along the light polarization vector. See, e.g., A. V. Efanov and M. V. Entin, Phys. Stat. Sol. (B) **118**, 63 (1983).

* Electronic address: lan.qing@rochester.edu

† Also at Department of Electrical and Computer Engineering, University of Rochester, Rochester, NY 14627.

[1] J. M. Luttinger and W. Kohn, Phys. Rev. **97**, 869 (1955).